Complex Rayleigh-Van Der Pol-Duffing Oscillators: Dynamics, Phase and Anti-Phase Synchronization

Gamal M. . Mahmoud , Ahmed A. Farghaly , Tarek M. Abed-Elhameed , Asma Al Themairi *

Posted Date: 9 November 2023

doi: 10.20944/preprints202311.0607.v1

Keywords: hyperchaotic; complex; Rayleigh-Van der Pol-duffing oscillator; phase synchronization; anti phase synchronization

Article

Complex Rayleigh-Van Der Pol-Duffing Oscillators: Dynamics, Phase and Anti-Phase Synchronization

Asma Al Themairi [1,*], Gamal M. Mahmoud [2], Ahmed A. Farghaly [2,3] and Tarek M. Abed-Elhameed [2]

[1] Department of Mathematical Sciences, College of Science, Princess Nourah bint Abdulrahman University,P.O.Box 84428, Riyadh 11671, Saudi Arabia
[2] Department of Mathematics, Faculty of Science, Assiut University, Assiut 71516, Egypt
[3] Department of Information Technology, College of Computer and Information Sciences, Majmaah University, Al-Majmaah 11952, Saudi Arabia
* Correspondence: aialthumairi@pnu.edu.sa

Abstract: This paper introduces the complex Rayleigh-van der Pol-Duffing oscillators (RVDOs), which are hyperchaotic and can be either autonomous or non-autonomous. The fundamental dynamics of the autonomous and non-autonomous complex RVDOs including dissipation, symmetry, fixed points and their stability are studied. These oscillators are found in various important fields of physics and engineering. The paper proposes a scheme to achieve phase synchronization (PS) and antiphase synchronization (APS) for different dimensional models. These kinds of synchronization are considered as generalization of several other types of synchronization. For this scheme we use the active control method based on Lyapunov stability theory. By analytically determining the control functions, the scheme achieved PS and APS. Our scheme is applied to study PS of hyperchaotic behaviors for two distinct hyperchaotic non-autonomous and autonomous complex RVDOs. Additionally, the scheme is employed to achieve APS of chaotic real non-autonomous RVDO and hyperchaotic complex autonomous RVDO, including those with different dimensions. Our work presents numerical results that plot the amplitudes and phases of these hyperchaotic behaviors, demonstrating the successful achievement of PS and APS.

Keywords: hyperchaotic; complex; rayleigh-van der pol-duffing oscillator; phase synchronization; anti-phase synchronization

0. Introduction

The phase and anti-phase synchronization of chaotic systems have gained significant interest because of their relevance to various fields and scenarios. These include lasers [1,2], complex networks [3], electrical circuits [4], memory processes [5], optical parametric oscillators [6], human cortex [7], fluids [8], neuroscience [9], ecological systems [10], coupled chemical oscillators [11], and the heartbeat and respiration cycle [12]. Many techniques to study the phase synchronization for the same dimension were introduced such as complete phase synchronization [13,14], anti-phase synchronization [14], modified projective phase synchronization [15] and combination-combination phase synchronization [16]. On the other hand, different kinds of synchronization were introduced in the literature [17,18] and the references therein. It is widely acknowledged that real-world models exhibit nonlinearity as a fundamental characteristic. Consequently, the dynamics of these models are mathematically depicted using nonlinear ODEs [19–21]. Kpomahou *et al.* [22] introduced the real **R**ayleigh-**v**an der Pol-**D**uffing **o**scillator (RVDO) as:

$$\ddot{u} - u + au^3 - e(b - cu^2 - d\dot{u}^2)\dot{u} + el(1 - au^2)ucos(2wt) = e(h + 2msin(\Omega t))cos(wt), \quad (1)$$

where the expression $-u + au^3 + el(1 - au^2)u\cos(2wt)$ represents the components of linear and nonlinear stiffness that contribute to the linear and nonlinear parametric excitation, $e(-b + cu^2 + d\dot{u}^2)\dot{u}$

Preprints (www.preprints.org) | NOT PEER-REVIEWED | Posted: 9 November 2023 doi:10.20944/preprints202311.0607.v1

is the hybrid Rayleigh-Van der Pol damping force and $e(h+2msin(\Omega t))cos(wt))$ is the external excitation force, w and Ω represent the two frequencies of the force that is modulated in amplitude, while $2m$, h, e stand for the degree of modulation, the unmodulated carrier amplitude and a small quantity characterizing the smallness of the dissipative and forced terms, respectively. If one put $v_1 = u, v_2 = \dot{u}$, the two first order ordinary differential equations of oscillator (1) are:

$$\begin{aligned} \dot{v}_1 &= v_2, \\ \dot{v}_2 &= v_1 - a{v_1}^3 + e(b - c{v_1}^2 - d{v_2}^2)v_2 - el(1 - a{v_1}^2)v_1 cos(2wt) + e(h + 2msin(\Omega t))cos(wt). \end{aligned} \tag{2}$$

If we consider that $v_1 = z_1 + iz_2$ and $v_2 = z_3 + iz_4$, $i = \sqrt{-1}$ are complex variables, then the 4D real form of RVDO (2) is:

$$\begin{aligned} \dot{z}_1 =& z_3, \\ \dot{z}_2 =& z_4, \\ \dot{z}_3 =& z_1 - a({z_1}^3 - 3z_1{z_2}^2) + e\{bz_3 - c[(z_1^2 - z_2^2)z_3 - 2z_1z_2z_4] - d[{z_3}^3 - 3z_3{z_4}^2]\} \\ & - el\{[1 - a(z_1^2 - z_2^2)]z_1 + 2az_1z_2^2\}cos(2wt) + e(h + 2msin(\Omega t))cos(wt), \\ \dot{z}_4 =& z_2 - a(-{z_2}^3 + 3z_1^2z_2)e\{bz_4 - c[(z_1^2 - z_2^2)z_4 + 2z_1z_2z_3] - d[-{z_4}^3 + 3z_3^2z_4]\} \\ & - el\{[1 - a(z_1^2 - z_2^2)]z_2 - 2az_1^2z_2\}cos(2wt). \end{aligned} \tag{3}$$

For the choice $l = h = m = 0$, the autonomous form of RVDO (3) is gives as:

$$\begin{aligned} \dot{z}_1 =& z_3, \\ \dot{z}_2 =& z_4, \\ \dot{z}_3 =& z_1 - a({z_1}^3 - 3z_1{z_2}^2) + e\{bz_3 - c[(z_1^2 - z_2^2)z_3 - 2z_1z_2z_4] - d[{z_3}^3 - 3z_3{z_4}^2]\} \\ \dot{z}_4 =& z_2 - a(-{z_2}^3 + 3z_1^2z_2) + e\{bz_4 - c[(z_1^2 - z_2^2)z_4 + 2z_1z_2z_3] - d[-{z_4}^3 + 3z_3^2z_4]\}. \end{aligned} \tag{4}$$

This paper introduces hyperchaotic non-autonomous and autonomous complex Rayleigh-van der Pol-Duffing oscillators (3) and (4), respectively. We investigate the basic dynamics for these oscillators including dissipation, symmetry, fixed points and their stability. Using the Lyapunov exponents [23], we prove that models (3) and (4) have hyperchaotic solutions. The paper proposes, also, a scheme utilizing an active control technique based on Lyapunov stability analysis to achieve phase synchronization (PS) and antiphase synchronization (APS) for different dimension models. According to the literature, these kinds of synchronization are a generalization of several other forms [14,15].

This paper is organized as follows: Section 1 contains the dynamics of the proposed complex oscillators (3-4) including fixed points and their stability, dissipation, symmetry and chaotic behavior. In Section 2, we introduce a scheme to achieve PS and APS based on active control technique and Lyapunov stability analysis. Sections 3 and 4 deal with illustrative examples for PS and APS, respectively. Section 5 presents our conclusions.

1. Dynamics of complex RVDOs (3-4)

This section presents the characteristics and behavior of our suggested autonomous RVDO (3) and nonautonomous RVDO (4). These models are dissipative under the condition $eb < 0$. It is clear that model (3) is not symmetric and model (4) is symmetric under the transformation $(z_1, z_2, z_3, z_4) \longrightarrow (-z_1, -z_2, -z_3, -z_4)$. Model RVDO (3) has not fixed points, while model (4) has three ones as:

Preprints (www.preprints.org) | NOT PEER-REVIEWED | Posted: 9 November 2023 doi:10.20944/preprints202311.0607.v1

$E_0 = (0,0,0,0)^T$ and $E_{1,2} = (\pm\frac{1}{\sqrt{a}},0,0,0)^T$ for $a > 0$. To study the stability of $E_0 = (0,0,0,0)^T$, we calculate the Jacobian matrix of the model (4) at E_0 as:

$$\begin{pmatrix} 0 & 0 & 1 & 0 \\ 0 & 0 & 0 & 1 \\ 1 & 0 & eb & 0 \\ 0 & 1 & 0 & eb \end{pmatrix}, \tag{5}$$

and its eigenvalues are: $\mu_{1,2} = \mu_{3,4} = \frac{be\pm\sqrt{b^2e^2+4}}{2}$. It is clear that E_0 is not stable for any values of the parameters e and b. The fixed points $E_{1,2}$ can be similarly study as we did for E_0.

For the choice, $a = 1.25$, $b = 0.5$, $c = 0.085$, $e = 1$, $h = 1$, $m = 0.5$, $l = 0.05$, $w = 1$, $\Omega = 1$ and calculating the Lyapunov exponents [23] for the real autonomous RVDO (2), the complex autonomous RVDO(3) and the complex nonautonomous RVDO (4). We found those values are $(\lambda_1 = 0.1556, \lambda_2 = 0, \lambda_3 = -0.4198)$, $(\lambda_{1,2} = 0.028, \lambda_3 = 0, \lambda_4 = -0.7289, \lambda_5 = -0.6709)$, and $(\lambda_{1,2} = 0.0878, \lambda_3 = -0.3291, \lambda_4 = -5.1644)$, respectively. This means that the real autonomous RVDO (2) has chaotic solution, the complex autonomous RVDO(3) has hyperchaotic solution of order 2 and the complex nonautonomous RVDO (4) has hyperchaotic solution of order 2 as shown in Figures 1–3.

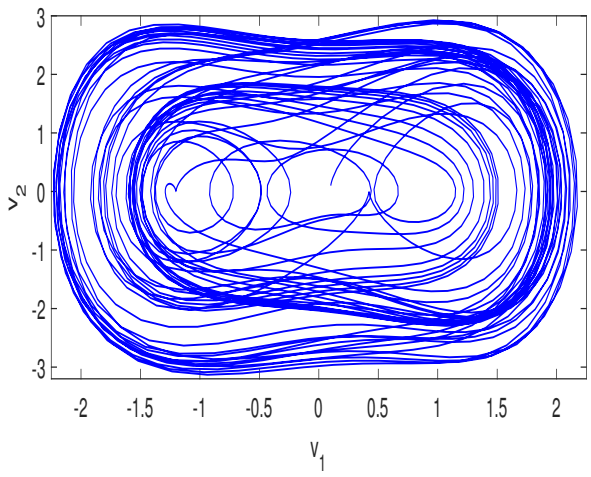

Figure 1. Chaotic solution of model RVDO (2) for $d = 0$ and the initial values $v_0 = (0.1, 0.1)^T$ in (v_1, v_2) space.

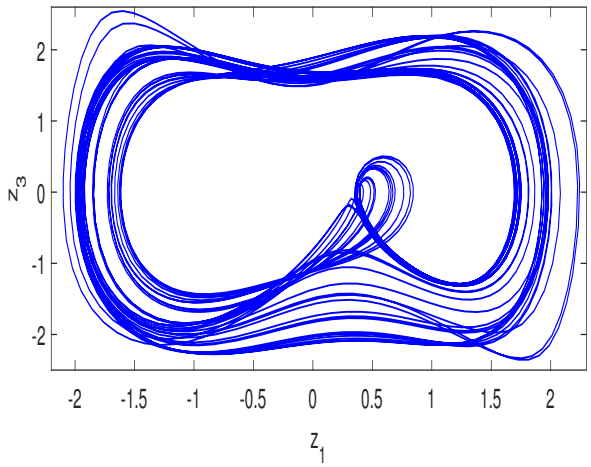

Figure 2. Hyperchaotic solution of model RVDO (3) for $d = 0.2$ and the initial values $z_0 = (0.1, 0.1, 0.1, 0.1)^T$ in (z_1, z_3) space.

Preprints (www.preprints.org) | NOT PEER-REVIEWED | Posted: 9 November 2023 doi:10.20944/preprints202311.0607.v1

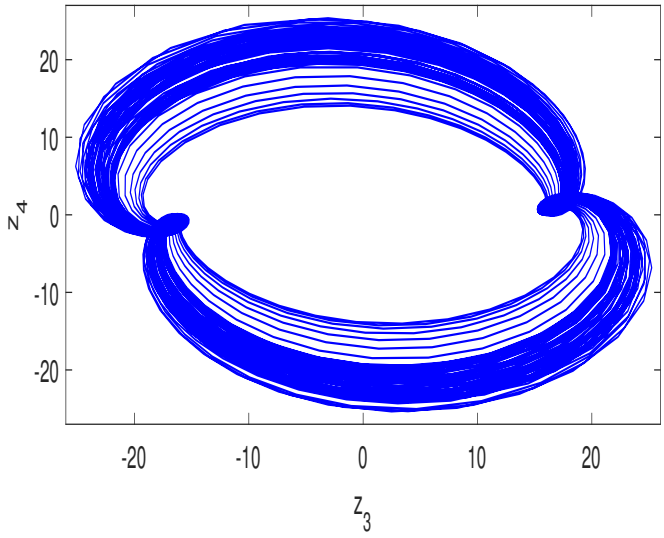

Figure 3. Hyperchaotic solution of model RVDO (4) for $d = 0$ and the initial values $z_0 = (0.1, 0.1, 0.1, 0.1)^T$ in (z_3, z_4) space.

In the following remarks, we will present the differences between models (2-4). Model (3) is considered a generalization of model (2). Model (3) is not symmetric and model (4) is symmetric. Model (4) has 3 fixed points, while model (3) does not. It is observed that the count of Lyapunov exponents in non-autonomous models is higher by one compared to autonomous models with the same dimensions. This difference arises due to the inclusion of time as an additional dimension in the non-autonomous models.

2. A scheme for PS and APS with different dimensions

In our plan, we make the assumption that there is a single master model and a single slave system. The master system represents:

$$\dot{z} = f(z, t), \tag{6}$$

while the slave model is:

$$\dot{\zeta} = g(\zeta, t) + u, \tag{7}$$

where $z \in R^n, \zeta \in R^m$ are the state vectors of models and $u \in R^m$ is the control function which will be calculated. PS can be observed in the master system (6) as well as the slave system (7), provided that there exist two constant matrices $A \in R^{n\times n}$, and $B \in R^{n\times m}$ in the real matrix space, if

$$\lim_{x\to\infty} \|E\| = \lim_{x\to\infty} \|B\zeta - Az\| = C, \tag{8}$$

where $E = (e_1, e_2, ..., e_n)^T \in R^n$ is the error vector, and C is a constant vector. The APS for different dimensions can be obtained if one takes $A = -A$ in Eq. (8). If $\zeta in R^n$ and $A = B = I \in R^{n\times n}$, then the PS for different dimensions converted to PS with the same dimensions [14]. The modified PS with the same dimensions can be get from Eq. (8), if one choose $\zeta in R^n$ and $B \in R^{n\times n}$ [15].

We can achieve PS among two distinct models (6-7), if we design the vector of the control functions $U \in R^n$ in the following way:

$$U \equiv Bu = Af(z, t) - Bg(\zeta, t) - KE, \tag{9}$$

Preprints (www.preprints.org) | NOT PEER-REVIEWED | Posted: 9 November 2023 doi:10.20944/preprints202311.0607.v1

where $K = diag(k_1, k_2, ..., k_n)$ is the control gain diagonal matrix.

Proof. From Eq. (8), we have

$$E = B\zeta - Az, \tag{10}$$

by taking the derivative of Equation (10) with respect to time, we derive the following expression:

$$\dot{E} = B\dot{\zeta} - A\dot{z}, \tag{11}$$

using Eqs. (6-7) and (9), we get

$$\dot{E} = -KE, \tag{12}$$

by utilizing Lyapunov stability analysis, if we assign K to be zero, Eq. (12) can be expressed in the following form $\dot{E} = 0$. This means that $E \longrightarrow C$ as $t \longrightarrow \infty$, then PS is achieved. □

For the choice $k_i < 0$ and using the stability theory, then $E \longrightarrow 0$ as $t \longrightarrow \infty$. According to Remark 2, the APS between the models (6-7) can be achieved if the control functions take the form:

$$U \equiv Bu = -Af(z,t) - Bg(\zeta,t) - KE. \tag{13}$$

The phase differences Δ_{ij} between the $\left(\sum_{k=1}^{n} A_{ik}z_k, \sum_{k=1}^{n} A_{jk}z_k\right)$ projection for the master model and the $\left(\sum_{l=1}^{m} B_{il}\zeta_l, \sum_{l=1}^{m} B_{jl}\zeta_l\right)$ projection for the slave one are described as follows:

$$\Delta_{ij} = \psi_{ij}^{d} - \psi_{ij}^{r}, \tag{14}$$

where $i, j = 1, 2, 3, ..., n$, $i \neq j$, $\psi_{ij}^{d} = tan^{-1}\left(\frac{\sum_{k=1}^{n} A_{jk}z_k}{\sum_{k=1}^{n} A_{ik}z_k}\right)$ and $\psi_{ij}^{r} = tan^{-1}\left(\frac{\sum_{l=1}^{m} B_{jl}\zeta_l}{\sum_{l=1}^{m} B_{il}\zeta_l}\right)$. The occurrence of the PS is dependent on the bounded nature of these phase differences.

The definitions of the amplitudes in the $\left(\sum_{k=1}^{n} A_{ik}z_k, \sum_{k=1}^{n} A_{jk}z_k\right)$ projection for the master model and the $\left(\sum_{l=1}^{m} B_{il}\zeta_l, \sum_{l=1}^{m} B_{jl}\zeta_l\right)$ projection for the slave one are as follows:

$$\begin{aligned} A_{ij}^{d} &= \sqrt{\left(\sum_{k=1}^{n} A_{ik}z_k\right)^2 + \left(\sum_{k=1}^{n} A_{jk}z_k\right)^2}, \\ A_{ij}^{r} &= \sqrt{\left(\sum_{l=1}^{m} B_{il}\zeta_l\right)^2 + \left(\sum_{l=1}^{m} B_{jl}\zeta_l\right)^2}. \end{aligned} \tag{15}$$

Subsequently, we utilize this approach to examine the occurrence of PS in Section 3 and APS in Section 4 by applying it to hyperchaotic attractors (2-4).

3. Illustrative example for PS

In this section, we test the PS technique using an example. We consider the model (3) as the master model and the slave one is model (4). The slave model can be written after adding the control functions as:

Preprints (www.preprints.org) | NOT PEER-REVIEWED | Posted: 9 November 2023 doi:10.20944/preprints202311.0607.v1

$$\begin{aligned}
\dot{\zeta}_1 =& \zeta_3 + u_1,\\
\dot{\zeta}_2 =& \zeta_4 + u_2,\\
\dot{\zeta}_3 =& \zeta_1 - a({\zeta_1}^3 - 3\zeta_1{\zeta_2}^2) + e\{b\zeta_3 - c[(\zeta_1^2 - \zeta_2^2)\zeta_3 - 2\zeta_1\zeta_2\zeta_4] - d[{\zeta_3}^3 - 3\zeta_3{\zeta_4}^2]\} + u_3,\\
\dot{\zeta}_4 =& \zeta_2 - a(-{\zeta_2}^3 + 3\zeta_1^2\zeta_2)e\{b\zeta_4 - c[(\zeta_1^2 - \zeta_2^2)\zeta_4 + 2\zeta_1\zeta_2\zeta_3] - d[-{\zeta_4}^3 + 3\zeta_3^2\zeta_4]\} + u_4,
\end{aligned} \tag{16}$$

where $u = (u_1, u_2, u_3, u_4)^T$ is the control functions.

For the choice $A = B = I_{4\times 4}$ and applying Theorem 2, the control functions (9) can be written as:

$$\begin{aligned}
U_1 \equiv u_1 =& z_3 - \zeta_3 - k_1e_1,\\
U_2 \equiv u_2 =& z_4 - \zeta_4 - k_2e_2,\\
U_3 \equiv u_3 =& z_1 - a({z_1}^3 - 3z_1{z_2}^2) + e\{bz_3 - c[(z_1^2 - z_2^2)z_3 - 2z_1z_2z_4] - d[{z_3}^3 - 3z_3{z_4}^2]\} - el\{[1 - a(z_1^2 - z_2^2)]z_1\\
&+ 2az_1z_2^2\}cos(2wt) + e(h + 2msin(\Omega t))cos(wt) - \zeta_1 + a({\zeta_1}^3 - 3\zeta_1{\zeta_2}^2) - e\{b\zeta_3 - c[(\zeta_1^2 - \zeta_2^2)\zeta_3\\
&- 2\zeta_1\zeta_2\zeta_4] - d[{\zeta_3}^3 - 3\zeta_3{\zeta_4}^2]\} - k_3e_3,\\
U_4 \equiv u_4 =& z_2 - a(-{z_2}^3 + 3z_1^2z_2)e\{bz_4 - c[(z_1^2 - z_2^2)z_4 + 2z_1z_2z_3] - d[-{z_4}^3 + 3z_3^2z_4]\} - el\{[1 - a(z_1^2 - z_2^2)]z_2\\
&- 2az_1^2z_2\}cos(2wt) - \zeta_2 + a(-{\zeta_2}^3 + 3\zeta_1^2\zeta_2) - e\{b\zeta_4 - c[(\zeta_1^2 - \zeta_2^2)\zeta_4 + 2\zeta_1\zeta_2\zeta_3] - d[-{\zeta_4}^3 + 3\zeta_3^2\zeta_4]\} - k_4e_4.
\end{aligned} \tag{17}$$

During the numerical simulation, we use the same parameters and initial conditions of the master and slave models (3) and (16) of Figures 2–3. For the choice $K = 0$, the results of PS are shown in Figures 4–6. Figures 4–5 show the phase differences for six plane projections versus t. The confirmation of achieving PS is supported by the observation that the phase differences remain within a bounded range. The amplitudes of the master and the slave models in (z_1, z_3) and (ζ_1, ζ_3) spaces (A^d_{13} and A^r_{13}) are shown in Figure 6 (a) and (b), and Figure 6 (c) displays A^d_{13} versus A^r_{13}. Figure 6 demonstrates that these amplitudes exhibit hyperchaotic behavior and are uncorrelated. Similar results are observed for the other amplitudes of the master and slave systems in different plane projections.
While for $K = diag(0.5, 2, 1.5, 1)$, the state variables for the master model (3) and the slave model (16) are shown in Figure 7. Figure 8 depicts the synchronization errors which are approach zero.

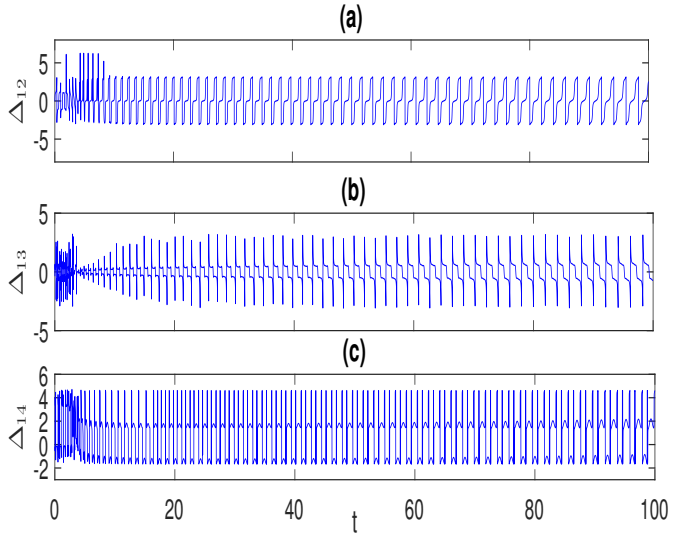

Figure 4. The phase differences of PS between the master model (3) and slave model (16) for different plane projections versus t: (a) Δ_{12} , (b) Δ_{13}, (c) Δ_{14}.

Preprints (www.preprints.org) | NOT PEER-REVIEWED | Posted: 9 November 2023 doi:10.20944/preprints202311.0607.v1

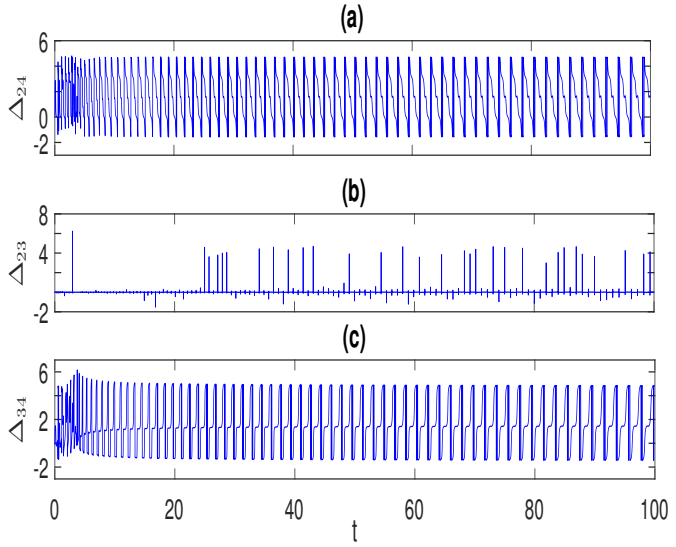

Figure 5. The phase differences of PS between the master model (3) and slave model (16) for different plane projections versus t: (a) Δ_{24} , (b) Δ_{23}, (c) Δ_{34}.

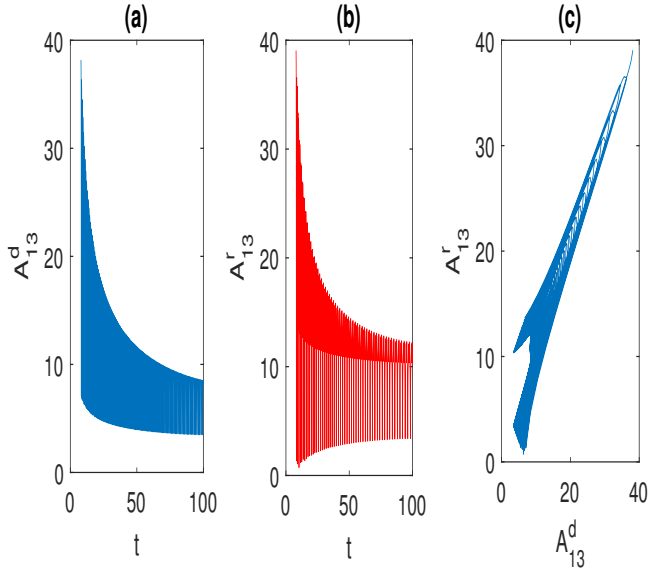

Figure 6. The amplitudes of the master and the slave models in (z_1, z_3) and (ζ_1, ζ_3) spaces: (a) A^d_{13} versus t, (b) A^r_{13} versus t, (c) (A^d_{13}, A^r_{13}) space.

Preprints (www.preprints.org) | NOT PEER-REVIEWED | Posted: 9 November 2023 doi:10.20944/preprints202311.0607.v1

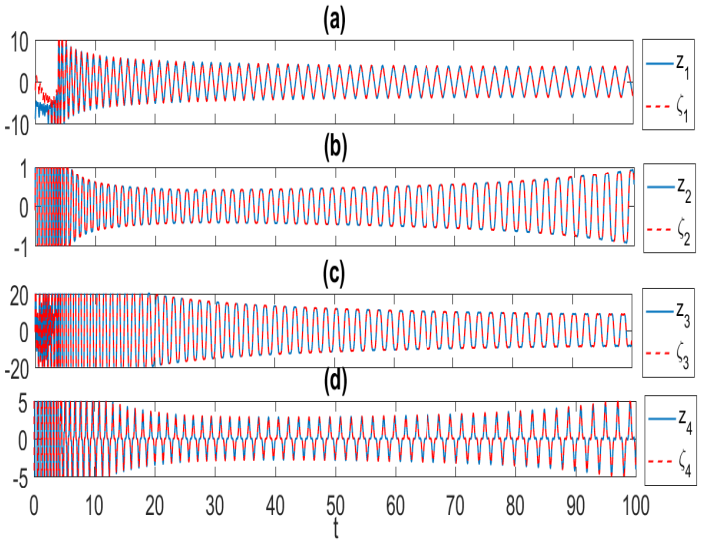

Figure 7. The state variables for the master model (3) and the slave model (16) after PS: (a) z_1 and ζ_1 versus t, (b) z_2 and ζ_2 versus t, (c) z_3 and ζ_3 versus t, (d) z_4 and ζ_4 versus t.

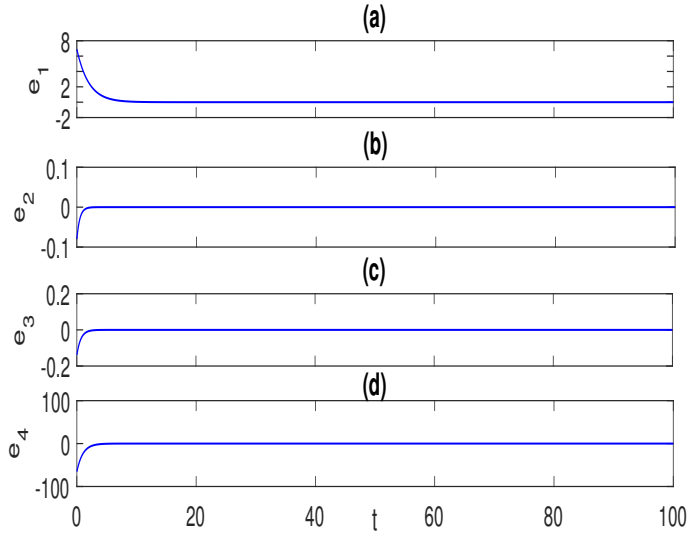

Figure 8. The synchronization errors of the master model (3) and the slave model (16): (a) e_1 versus t, (b) e_2 versus t, (c) e_3 versus t, (d) e_4 versus t.

4. Illustrative example for APS

In this section, we introduce an example for APS with different dimensions. We consider the model (2) as the 2D master model and model (16) is the 4D slave one.

For the choice $A = I_{2\times 2}$ and $B = \begin{pmatrix} 1 & 0 & 1 & 0 \\ 0 & 1 & 0 & 1 \end{pmatrix}$ and applying Corollary 2, the control functions (13) can be written as:

$$\begin{aligned} U_1 \equiv u_1 + u_3 &= -v_2 - \zeta_3 - (\zeta_1 - a({\zeta_1}^3 - 3\zeta_1{\zeta_2}^2) + e\{b\zeta_3 - c[(\zeta_1^2 - \zeta_2^2)\zeta_3 - 2\zeta_1\zeta_2\zeta_4] - d[{\zeta_3}^3 - 3\zeta_3{\zeta_4}^2]\} + u_3) - k_1e_1, \\ U_2 \equiv u_2 + u_4 &= -(v_1 - a{v_1}^3 + e(b - c{v_1}^2 - d{v_2}^2)v_2 - el(1 - a{v_1}^2)v_1 cos(2wt) + e(h + 2msin(\Omega t))cos(wt)) \\ &\quad - \zeta_4 - (\zeta_2 - a(-{\zeta_2}^3 + 3\zeta_1^2\zeta_2)e\{b\zeta_4 - c[(\zeta_1^2 - \zeta_2^2)\zeta_4 + 2\zeta_1\zeta_2\zeta_3] - d[-{\zeta_4}^3 + 3\zeta_3^2\zeta_4]\}) - k_2e_2. \end{aligned} \tag{18}$$

In the numerical simulation, we use the same parameters and initial conditions of the master and slave models (2) and (16) of Figures 1 and 3. For the choice $K = 0$, the results of PS are shown in

Preprints (www.preprints.org) | NOT PEER-REVIEWED | Posted: 9 November 2023 doi:10.20944/preprints202311.0607.v1

Figures 9 and 10. Figure 9 depicts the phase differences for one plane projections versus t. The fact that the phase differences are bounded confirms the achievement of PS. The amplitudes of the master and the slave models in (v_1, v_2) and $(\zeta_1 + \zeta_3, \zeta_2 + \zeta_4)$ spaces (A^d_{12} and A^r_{12}) are shown in Figure 10 (a) and (b), and Figure 6 (c) displays A^d_{12} versus A^r_{12}. Figure 10 demonstrates that these amplitudes exhibit hyperchaotic behavior and are uncorrelated (linearly independent).
While for $K = diag(0.5, 2)$, the state variables for the master model (2) and the slave model (16) are shown in Figure 11. Figure 12 depicts the synchronization errors which are approach zero.

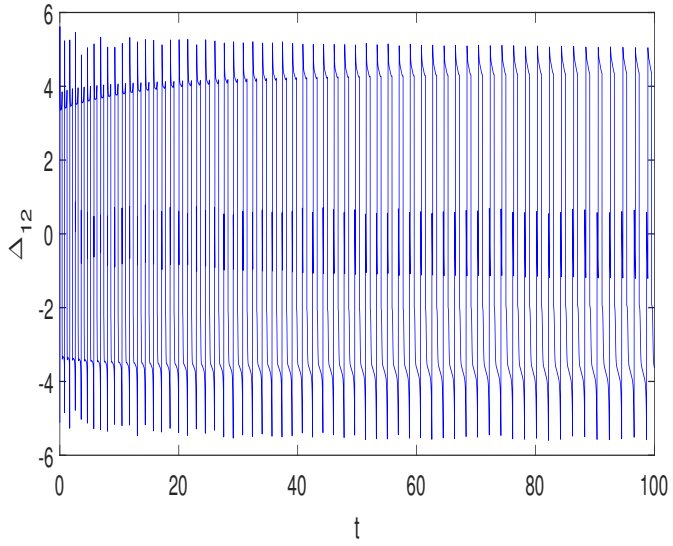

Figure 9. The phase differences of APS between the master model (2) and slave model (16) for the projection (v_1, v_2) versus t.

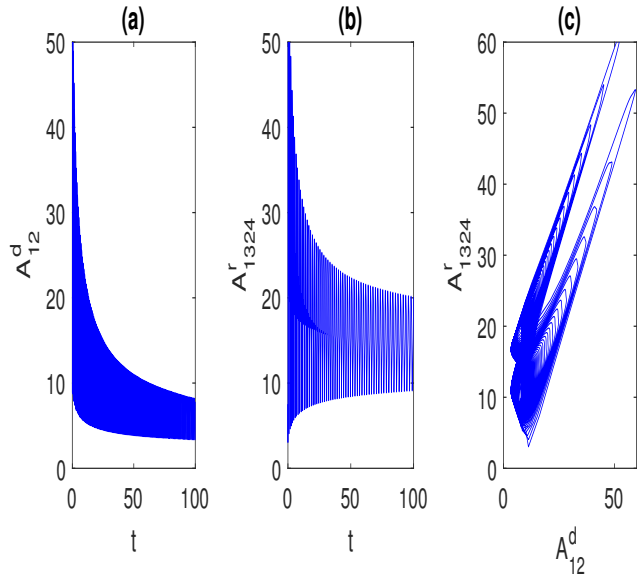

Figure 10. The amplitudes of the master model (2) and the slave model (16) in (v_1, v_2) and $(\zeta_1 + \zeta_3, \zeta_2 + \zeta_4)$ spaces: (a) A^d_{12} versus t, (b) A^r_{1324} versus t, (c) (A^d_{12}, A^r_{1324}) space.

Preprints (www.preprints.org) | NOT PEER-REVIEWED | Posted: 9 November 2023 doi:10.20944/preprints202311.0607.v1

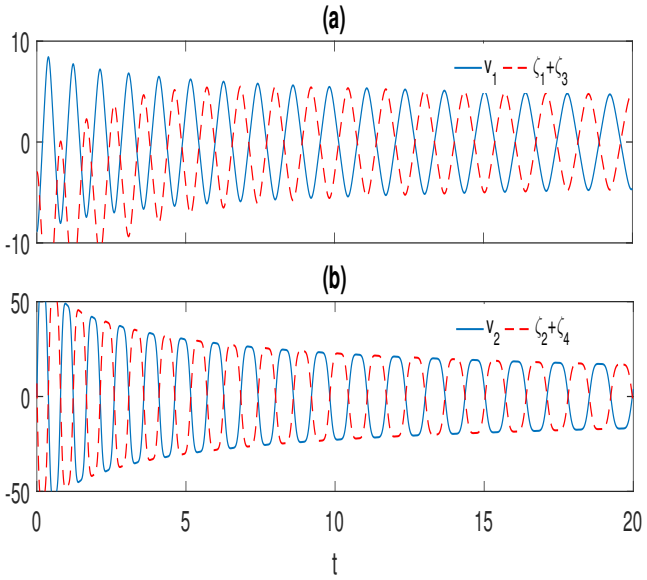

Figure 11. The state variables for the master model (2) and the slave model (16) after APS: (a) v_1 and $\zeta_1 + \zeta_3$ versus t, (b) v_2 and $\zeta_2 + \zeta_4$ versus t.

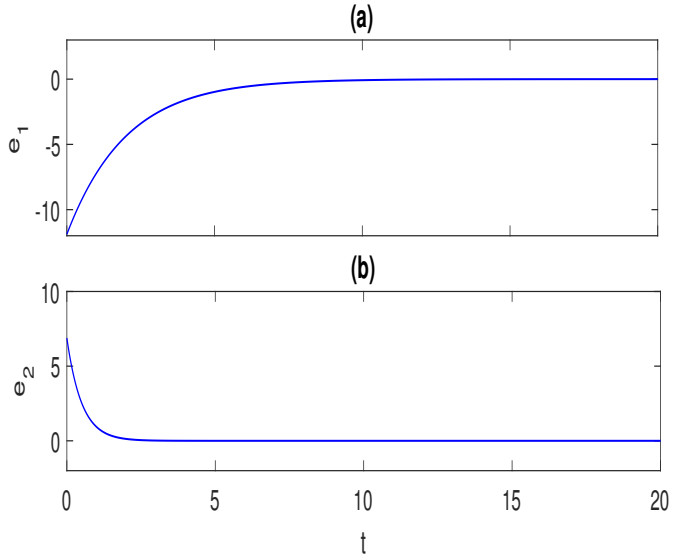

Figure 12. The synchronization errors of the master model (2) and the slave model (16): (a) e_1 versus t, (b) e_2 versus t.

5. Conclusion

In conclusion, this paper has introduced the hyperchaotic non-autonomous and autonomous complex Rayleigh-van der Pol-Duffing oscillators (RVDOs) (3) and (4). We studied into the fundamental dynamics of these oscillators, such as stability, fixed points, and dissipation. We demonstrated the hyperchaotic solutions of models (3) and (4) using the Lyapunov exponents and are shown in Figures 1–3. The hyperchaotic nature of these models may be used in numerous significant engineering and scientific domains. The proposed scheme in Section 2, utilizing an active control technique based on Lyapunov stability analysis, aims to achieve PS and APS for different dimensional models. Through the analytical determination of control functions (9) and (13), the scheme successfully achieved PS and APS. These types of synchronization are considered a generalization of many types in the literature [14,15]. The scheme is applied to investigate PS of hyperchaotic attractors (3) and (4). As well as to achieve APS, we used the models (2) and (4) including those with different dimensions. The

presented numerical results illustrating the phases and amplitudes of these chaotic and hyperchaotic attractors, and provide evidence of the effective accomplishment of PS and APS. These results are shown in Figures 4–12.

Funding: Funding for this manuscript was provided by Princess Nourah bint Abdulrahman University Researchers Supporting Project number (PNURSP2023R295).

Data Availability Statement: No data were used to support this study.

Acknowledgments: Princess Nourah bint Abdulrahman University Researchers Supporting Project number (PNURSP2023R295) Princess Nourah bint Abdulrahman University,Riyadh,Saudi Arabia.

Conflicts of Interest: The authors declare no conflicts of interest.

References

1. Hillbrand, J.; Auth, D.; Piccardo, M.; Opačak, N.; Gornik, E.; Strasser, G.; Capasso, F.; Breuer, S.; Schwarz, B. In-phase and anti-phase synchronization in a laser frequency comb. *Physical review letters* **2020**, *124*, 023901.
2. Mao, X.; Sun, Y.; Wang, L.; Guo, Y.; Gao, Z.; Wang, Y.; Li, S.; Yan, L.; Wang, A. Instability of optical phase synchronization between chaotic semiconductor lasers. *Optics Letters* **2021**, *46*, 2824–2827.
3. Dörfler, F.; Bullo, F. Synchronization in complex networks of phase oscillators: A survey. *Automatica* **2014**, *50*, 1539–1564. doi:https://doi.org/10.1016/j.automatica.2014.04.012.
4. Xie, Y.; Yao, Z.; Ma, J. Phase synchronization and energy balance between neurons. *Frontiers of Information Technology & Electronic Engineering* **2022**, *23*, 1407–1420.
5. Fell, J.; Axmacher, N. The role of phase synchronization in memory processes. *Nature reviews neuroscience* **2011**, *12*, 105–118.
6. Xiu-Qin, F.; Ke, S. Phase synchronization and anti-phase synchronization of chaos for degenerate optical parametric oscillator. *Chinese Physics* **2005**, *14*, 1526.
7. Arnulfo, G.; Wang, S.H.; Myrov, V.; Toselli, B.; Hirvonen, J.; Fato, M.; Nobili, L.; Cardinale, F.; Rubino, A.; Zhigalov, A.; others. Long-range phase synchronization of high-frequency oscillations in human cortex. *Nature communications* **2020**, *11*, 5363.
8. Chakrabarti, B.; Shelley, M.J.; Fürthauer, S. Collective Motion and Pattern Formation in Phase-Synchronizing Active Fluids. *Physical Review Letters* **2023**, *130*, 128202.
9. Tallon-Baudry, C.; Bertrand, O.; Delpuech, C.; Pernier, J. Stimulus specificity of phase-locked and non-phase-locked 40 Hz visual responses in human. *Journal of Neuroscience* **1996**, *16*, 4240–4249.
10. Blasius, B.; Huppert, A.; Stone, L. Complex dynamics and phase synchronization in spatially extended ecological systems. *Nature* **1999**, *399*, 354–359.
11. Totz, J.F.; Snari, R.; Yengi, D.; Tinsley, M.R.; Engel, H.; Showalter, K. Phase-lag synchronization in networks of coupled chemical oscillators. *Physical Review E* **2015**, *92*, 022819.
12. Kurths, J.; Schäfer, C.; Rosenblum, M.; Abel, H.H. Synchronization in Human Cardiorespiratory System. APS March Meeting Abstracts, 1998, pp. Q12–05.
13. Shi, Y.; Li, T.; Zhu, J. Complete Phase Synchronization of Nonidentical High-Dimensional Kuramoto Model. *Journal of Statistical Physics* **2023**, *190*, 6.
14. Mahmoud, G.M.; Mahmoud, E.E. Phase and antiphase synchronization of two identical hyperchaotic complex nonlinear systems. *Nonlinear Dynamics* **2010**, *61*, 141–152.
15. Mahmoud, E.E. Modified projective phase synchronization of chaotic complex nonlinear systems. *Mathematics and Computers in Simulation* **2013**, *89*, 69–85.
16. Yadav, V.K.; Prasad, G.; Srivastava, M.; Das, S. Combination–combination phase synchronization among non-identical fractional order complex chaotic systems via nonlinear control. *International Journal of Dynamics and Control* **2019**, *7*, 330–340.
17. Mahmoud, G.M.; Ahmed, M.E.; Abed-Elhameed, T.M. On fractional-order hyperchaotic complex systems and their generalized function projective combination synchronization. *Optik* **2017**, *130*, 398–406.
18. Boccaletti, S.; Kurths, J.; Osipov, G.; Valladares, D.; Zhou, C. The synchronization of chaotic systems. *Physics reports* **2002**, *366*, 1–101.

19. Kpomahou, Y.; Adéchinan, J.; Hinvi, L. Effects of quartic nonlinearities and constant excitation force on nonlinear dynamics of plasma oscillations modeled by a Liénard-type oscillator with asymmetric double well potential. *Indian Journal of Physics* **2022**, *96*, 3247–3266.
20. Mahmoud, G.M.; Abed-Elhameed, T.M.; Elbadry, M.M. A class of different fractional-order chaotic (hyperchaotic) complex duffing-van der pol models and their circuits implementations. *Journal of Computational and Nonlinear Dynamics* **2021**, *16*, 121005.
21. Mahmoud, G.M.; Abed-Elhameed, T.M.; Khalaf, H. On fractional and distributed order hyperchaotic systems with line and parabola of equilibrium points and their synchronization. *Physica Scripta* **2021**, *96*, 115201.
22. Kpomahou, Y.; Agbélélé, K.; Tokpohozin, N.; Yamadjako, A. Influence of Amplitude-Modulated Force and Nonlinear Dissipation on Chaotic Motions in a Parametrically Excited Hybrid Rayleigh–Van der Pol–Duffing Oscillator. *International Journal of Bifurcation and Chaos* **2023**, *33*, 2330006.
23. Wolf, A.; Swift, J.B.; Swinney, H.L.; Vastano, J.A. Determining Lyapunov exponents from a time series. *Physica D: nonlinear phenomena* **1985**, *16*, 285–317.